

Fire-hose instability of inhomogeneous plasma flows with heat fluxes

E. S. Uchava,^{1,2,3} A. G. Tevzadze,^{4,2, a)} B. M. Shergelashvili,^{5,6,2} N. S. Dzhililov,⁷ and S. Poedts^{8,9}

¹⁾*Faculty of Exact and Natural Sciences, Tbilisi State University, Tbilisi, 0179, Georgia*

²⁾*Evgeni Kharadze Georgian National Astrophysical Observatory, Abastumani, 0301, Georgia*

³⁾*Nodia Institute of Geophysics, Tbilisi State University, Tbilisi, 0171, Georgia*

⁴⁾*Kutaisi International University, Kutaisi University Campus, Kutaisi, 4600, Georgia*

⁵⁾*Space Research Institute, Austrian Academy of Sciences, 8042, Graz, Austria*

⁶⁾*Centre for Computational Helio Studies, Faculty of Natural Sciences and Medicine, Ilia State University, 0162, Georgia*

⁷⁾*Shamakhy Astrophysical Observatory of the ANAS, Baku AZ-1000, Azerbaijan*

⁸⁾*Center for Mathematical Plasma Astrophysics, KU Leuven, B-3001, Leuven, Belgium*

⁹⁾*Institute of Physics, University of Maria Curie-Skłodowska, PL-20-031 Lublin, Poland*

We study the effects of heat flows and velocity shear on the parallel firehose instability in weakly collisional plasma flow. For this purpose we apply an anisotropic 16-moment MHD fluid closure model that takes into account the pressure and temperature anisotropy, as well as the effect of anisotropic heat flux. The linear stability analysis of the firehose modes is carried out in the incompressible limit, where the MHD flow is parallel to the background magnetic field, while the velocity is sheared in the direction transverse to the flow direction. It seems that an increase of the velocity shear parameter leads to higher growth rates of the firehose instability. The increase of the instability growth rate is most profound for perturbations with oblique wave-numbers $k_{\perp}/k_{\parallel} < 1$. Combined action of the velocity shear and heat fluxes introduce an asymmetry of the instability growth in the shear plane: perturbations with wave-vectors with a component in the direction of the velocity shear grow significantly stronger as compared to those with components in the opposite direction. We discuss the implications of the presented study on the observable features of the solar wind and possible measurements of local parameters of the solar wind based on the stability constraints set by the firehose instability.

I. INTRODUCTION

It is well known that in low density, ionized, rarefied flows, magnetic field effects can dominate over the particle collision effects. Such systems can exhibit different values of temperature and pressure when measured along and normal to the direction of the background magnetic field. In such flows the anisotropic effect of the gyration of the charged particles around magnetic field lines dominates over the isotropic particle collision process leading to a plasma with anisotropic thermodynamic properties.

Anisotropic ionized flows are prone to a number of kinetic instabilities that tap energy from the magnetic anisotropy and grow due to various destabilization mechanisms. Flows where the thermal energy dominates over the magnetic energy are prone to the firehose instability¹⁻⁵. When the pressure parallel to the magnetic field is sufficiently higher than the perpendicular pressure, transverse kink perturbations of the magnetic field can become unstable and grow exponentially in time. Also, it has been shown that in viscous dissipation, anisotropy plays a significant role in the heating of the solar coronal plasma shear flows⁶, even when other effects are abandoned.

The firehose instability has gained much attention recently⁷⁻¹⁵, since it is believed to be one of the primary kinetic instabilities affecting the solar and stellar wind dynamics. The importance of the firehose instability in various astrophysical situations is also recognized¹³. Still, much of the

observational evidence about the development of the instability comes from the measurements of pressure anisotropies in solar wind fluctuations¹⁶⁻²⁰.

It has been shown that the nonlinear development of the microscopic firehose instability can affect the large-scale dynamics of astrophysical plasmas²¹. A more detailed analysis of the instability development at nonlinear amplitudes can be conducted by means of numerical simulations^{13,22}. Moreover, direct numerical simulations of the classical firehose instability using a hybrid-kinetic numerical approximation confirm the predictions of the standard linear theory on the exponentially growing instability²³. In the isotropic limit, the plasma non-equilibrium thermalization manifested by periodic or rapid aperiodic variations of the system entropy in time, leads to strong coupling of different MHD wave modes (described in a similar mathematical framework as for waves in shear flows) and also to development of parametric instabilities²⁴.

The theoretical framework for many of the advances in the analysis of magnetically anisotropic flows using a fluid description, is adopting the Chew-Goldberger-Low (CGL) approximation²⁵. This limit exploits the simplicity of a fluid description by using a closure model that leads to two different equations of state, viz. parallel and perpendicular to the magnetic field. Thus, the CGL limit is often referred to as a double adiabatic anisotropic MHD description.

The purpose of the present paper is to study the properties of the firehose instability in weakly magnetized anisotropic shear flows with heat fluxes. Waves and instabilities of anisotropic MHD shear flows have been studied in the framework of the non-modal approach in the CGL limit²⁶. The CGL closure model neglects heat fluxes as low frequency phenom-

^{a)}Corresponding author: aleko@tevza.org

ena and uses the double adiabatic approximation for the analysis of higher frequency modes. On the other hand, the velocity shear of the flow is acting on the shearing time-scales: these time-scales are usually much longer than the short time scales described within the CGL limit and are comparable to the time scales of thermal processes. Therefore, we here employ a so-called 16-moment anisotropic MHD model that can be effectively used to analyze low frequency phenomena in such flows^{28,29}. This approximation enables us to study anisotropic plasmas with heat fluxes using the fluid description. The method is an extension of the 13-moment Grad method³⁰ for the case, taking into account higher order dispersive effects. These include two anisotropic heat flux vectors that describe transport of parallel and perpendicular thermal energies and viscosity tensor that describes collision-free viscosity effect. Viscous contribution can be often neglected in low frequency limit thus leading to the fluid model that represents apparent generalization of CGL-MHD model with addition of anisotropic heat fluxes. Indeed, the 16-moment formalism has already proven to be successful in analyzing waves and instabilities in weakly collisional media³¹⁻³⁵.

In this paper, we present the stability analysis of the low frequency incompressible perturbations to the anisotropic MHD shear flows with heat fluxes. Effects of the velocity shear and heat fluxes on the dynamics of linear perturbations are characterized by lower frequency compared to the compressibility effects. Thus, we adopt incompressibility approximation and study the properties of fire-hose instability when compressibility effects can not directly affect this instability in the linear limit.

The physical model of the problem is described in Sec. 2, where the steady-state flow is described. Section 3 presents the linear perturbations and the stability analysis of both static case as well as sheared flows are described, respectively. The effects of the velocity shear and anisotropic heat fluxes are summarized in Sec. 3.

II. PHYSICAL MODEL

The incompressible anisotropic MHD system can be described in the 16-moment approximation by using the following simplified fluid model^{28,29,34}:

$$\frac{d\mathbf{V}}{dt} + \frac{\nabla P_{\perp}}{\rho} + \frac{\mathbf{B} \times (\nabla \times \mathbf{B})}{4\pi\rho} = \frac{\nabla_{\parallel}}{\rho} \left((P_{\perp} - P_{\parallel}) \frac{\mathbf{B}}{B^2} \right), \quad (1)$$

$$\frac{d\mathbf{B}}{dt} - \nabla_{\parallel} \mathbf{V} = 0, \quad (2)$$

$$\nabla \cdot \mathbf{B} = 0, \quad (3)$$

and the incompressibility condition:

$$\nabla \cdot \mathbf{V} = 0, \quad (4)$$

where the following notations are used for the shortness:

$$d/dt \equiv \partial/\partial t + \mathbf{V} \cdot \nabla,$$

$$\nabla_{\parallel} \equiv \frac{\mathbf{B} \cdot \nabla}{B}.$$

The equations of state in the parallel and perpendicular to the magnetic field directions now include the heat fluxes:

$$\frac{d}{dt} \left(\frac{P_{\parallel} B^2}{\rho^3} \right) = -\frac{B^2}{\rho^3} \left(\nabla_{\parallel} \left(\frac{S_{\parallel}}{B} \right) + \frac{2S_{\perp}}{B^2} \nabla_{\parallel} B \right), \quad (5)$$

and

$$\frac{d}{dt} \left(\frac{P_{\perp}}{\rho B} \right) = -\frac{B^2}{\rho} \nabla_{\parallel} \left(\frac{S_{\perp}}{B^2} \right). \quad (6)$$

The CGL MHD equations can be derived by setting the heat flux parameters to zero ($S_{\perp} = S_{\parallel} = 0$) in Eqs. (5) and (6). The full closure of the system of Eqs.(1-6) can be accomplished through the 16-moment closure model that provides two more equations for the heat fluxes, namely:

$$\frac{d}{dt} \left(\frac{S_{\parallel} B^3}{\rho^4} \right) = -\frac{3P_{\parallel} B^2}{\rho^4} \nabla_{\parallel} \left(\frac{P_{\parallel}}{\rho} \right), \quad (7)$$

and

$$\frac{d}{dt} \left(\frac{S_{\perp}}{\rho^2} \right) = -\frac{P_{\parallel}}{B\rho^2} \left(\nabla_{\parallel} \left(\frac{P_{\perp}}{\rho} \right) + \frac{P_{\perp}}{\rho} \frac{P_{\perp} - P_{\parallel}}{P_{\parallel} B} \nabla_{\parallel} B \right). \quad (8)$$

For the sake of completeness we show connection between the fluid velocity of the flow \mathbf{V} and the velocity of individual particles \mathbf{u} in the kinetic regime using particle distribution function $f(\mathbf{u}, \mathbf{r}, t)$:

$$\mathbf{V} = \left(\int \mathbf{u} f d^3\mathbf{u} \right) / \left(\int f d^3\mathbf{u} \right).$$

Hence, parallel and perpendicular heat fluxes can be defined using the third moments as follows:

$$S_{\parallel} = \frac{m}{2B^2} \int d^3\mathbf{u} (\mathbf{u} \cdot \mathbf{B})^2 u_{\parallel} f,$$

$$S_{\perp} = \frac{m}{2} \int d^3\mathbf{u} \left(u^2 - \frac{(\mathbf{u} \cdot \mathbf{B})^2}{B^2} \right) u_{\perp} f,$$

where m and \mathbf{u} are mass and velocity of individual particles, while u_{\parallel} and u_{\perp} stand for the particle velocity components parallel and perpendicular to the magnetic field, respectively.

A. Steady-state equilibrium flow

We consider a stationary, weakly collisional MHD flow parallel to the uniform background magnetic field in the x -direction, with a velocity profile that is sheared linearly in the transverse (y -)direction:

$$\mathbf{V}_0 = (Ay, 0, 0), \quad \mathbf{B}_0 = (B_0, 0, 0), \quad (9)$$

where A is the transverse shear parameter of the parallel velocity. Assuming the similar physical origins of the pressure

and heat flux anisotropy in the rarefied flow, we introduce the pressure anisotropy parameter as follows:

$$\alpha = P_{\perp 0}/P_{\parallel 0} = S_{\perp 0}/S_{\parallel 0}. \quad (10)$$

The pressure and heat flux anisotropy parameters may be different due to the contribution from different plasma species (e.g., protons and electrons). Still, we neglect these differences within adopted one fluid description and use pressure anisotropy parameter as a guiding anisotropy factor for farther analysis. Described flow matches the average configuration of the solar and stellar winds locally, where the flow convexity and turbulent component can be neglected. Indeed it is known that, while being stable global configurations, such flows can exhibit a number of micro-instabilities depending on the magnetic field, anisotropy and heat flux parameters.

III. LINEAR STABILITY ANALYSIS

For the purpose of the stability analysis, we introduce linear perturbations of the background incompressible parallel shear flow embedded in a uniform magnetic field as follows:

$$\begin{aligned} \mathbf{V} &= \mathbf{V}_0 + \mathbf{V}', & \mathbf{B} &= \mathbf{B}_0 + \mathbf{B}', \\ P_{\parallel} &= P_{0\parallel} + P'_{\parallel}, & P_{\perp} &= P_{0\perp} + P'_{\perp}, \\ S_{\parallel} &= S_{0\parallel} + S'_{\parallel}, & S_{\perp} &= S_{0\perp} + S'_{\perp}, \end{aligned} \quad (11)$$

where $\mathbf{V}' \ll \mathbf{V}_0$, $\mathbf{B}' \ll \mathbf{B}_0$, etc., ρ is uniform constant density and

$$C_{\parallel}^2 \equiv P_{0\parallel}/\rho, \quad C_{\perp}^2 \equiv P_{0\perp}/\rho. \quad (12)$$

In present paper we study the effect of background stationary heat fluxes on the stability of local fire-hose instability. Thus, we introduce linear perturbations over the nonzero heat fluxes:

$$S_{0\parallel} \neq 0, \quad S_{0\perp} \neq 0.$$

Defining the Alfvén velocity as

$$V_A = B_0/\sqrt{4\pi\rho}, \quad (13)$$

we may introduce parallel and perpendicular plasma beta parameters as follows:

$$\beta_{\parallel} = 4\pi P_{0\parallel}/B_0^2, \quad \beta_{\perp} = 4\pi P_{0\perp}/B_0^2. \quad (14)$$

Effects of the heat fluxes can be described by the non-dimensional heat flux parameters³⁴:

$$\gamma_{\parallel} = \rho S_{0\parallel}/P_{0\parallel}^2, \quad \gamma_{\perp} = \rho S_{0\perp}/P_{0\perp}^2. \quad (15)$$

In the present paper, we introduce parallel and perpendicular heat flux parameters that also account for the magnetic field of the plasma:

$$q_{\parallel} = 2\gamma_{\parallel}\beta_{\parallel}^{1/2}, \quad q_{\perp} = 2\gamma_{\perp}\beta_{\perp}^{1/2}. \quad (16)$$

Hence, upon substituting Eqs. (12) into the Eqs. (1-6) and neglecting all the nonlinear terms, we can obtain the linear

system of partial differential equations describing the dynamics of perturbations in the anisotropic MHD flow. This system can be analyzed in the shearing sheet limit, where spatial Fourier expansion with time dependent wave-numbers can be employed as follows:

$$\begin{pmatrix} P'_{\parallel}(\mathbf{r}, t)/P_{0\parallel} \\ P'_{\perp}(\mathbf{r}, t)/P_{0\perp} \\ S'_{\parallel}(\mathbf{r}, t)/P_{0\parallel} \\ S'_{\perp}(\mathbf{r}, t)/P_{0\perp} \\ \mathbf{V}'(\mathbf{r}, t)/V_A \\ \mathbf{B}'(\mathbf{r}, t)/B_0 \end{pmatrix} \propto \begin{pmatrix} ip_{\parallel}(\mathbf{k}, \tau) \\ ip_{\perp}(\mathbf{k}, \tau) \\ s_{\parallel}(\mathbf{k}, \tau) \\ s_{\perp}(\mathbf{k}, \tau) \\ \mathbf{v}(\mathbf{k}, \tau) \\ i\mathbf{b}(\mathbf{k}, \tau) \end{pmatrix} \exp\left(i\mathbf{k}(\tau)\frac{\mathbf{r}}{L}\right). \quad (17)$$

Here, L corresponds to the characteristic length-scale of the flow, τ is the non-dimensional time variable

$$\tau = tV_A/L, \quad (18)$$

$k_y(\tau)$ is the non-dimensional shearing wave-number of the perturbation harmonics:

$$k_y(\tau) = k_{y0} - Rk_x\tau,$$

and R is the normalized velocity shear parameter

$$R = AL/V_A.$$

Spatial Fourier Harmonics of the physical quantities (p_{\parallel} , p_{\perp} , s_{\parallel} , s_{\perp} , etc.) derived from Eqs. (17) are in general a complex valued functions. Still, there are specific phase difference between different quantities on the complex plane. In uniform compressible flow without heat fluxes the phase of pressure and velocity perturbations differ by $\pi/2$. This means that perturbations with real valued velocity harmonics will have purely complex pressure harmonics. To account for these standard differences we introduce velocity and heat flux harmonics with real and pressure and magnetic field harmonics with purely complex factors (see Eq. 17).

In this framework we may derive the system of differential equations governing the linear dynamics of perturbation harmonics of the incompressible anisotropic shear flow system:

$$\dot{v}_x(\tau) = Rv_y(\tau) - \beta_{\perp}\frac{k_{\perp}^2}{k_x}p_{\perp}(\tau) - \frac{\Delta\beta k_x^2 + k^2}{k_x}b_x(\tau), \quad (19)$$

$$\dot{v}_y(\tau) = \beta_{\perp}k_y p_{\perp}(\tau) + k_y b_x(\tau) - (1 + \Delta\beta)k_x b_y(\tau), \quad (20)$$

$$\dot{p}_{\perp}(\tau) = k_x v_x(\tau) + Rb_y(\tau) - k_x s_{\perp}(\tau) + iq_{\perp}\alpha k_x b_x(\tau), \quad (21)$$

$$\begin{aligned} \dot{s}_{\parallel}(\tau) &= -\frac{3iq_{\parallel}}{2}k_x v_x(\tau) + 6Rv_y(\tau) - 3\beta_{\perp}\frac{k_{\perp}^2}{k_x}p_{\perp}(\tau) - \\ &\quad - 3\frac{2\Delta\beta k_x^2 + k^2}{k_x}b_x(\tau) - \frac{3iq_{\parallel}}{2}Rb_y(\tau), \end{aligned} \quad (22)$$

$$\dot{s}_{\perp}(\tau) = \beta_{\parallel}k_x p_{\perp}(\tau) + \Delta\beta k_x b_x(\tau), \quad (23)$$

$$\dot{b}_x(\tau) = Rb_y(\tau) + k_x v_x(\tau), \quad (24)$$

$$\dot{b}_y(\tau) = k_x v_y(\tau), \quad (25)$$

$$0 = k_x b_x(\tau) + k_y b_y(\tau) + k_z b_z(\tau). \quad (26)$$

where

$$\begin{aligned} k_{\perp}^2 &= k_y^2 + k_z^2, \\ k^2 &= k_x^2 + k_{\perp}^2, \\ \Delta\beta &\equiv \beta_{\perp} - \beta_{\parallel}, \end{aligned} \quad (27)$$

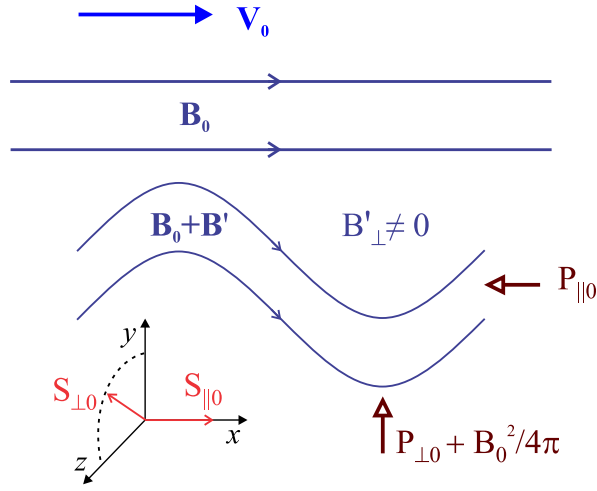


FIG. 1. Sketch illustration of the firehose instability in the flow parallel to the magnetic field. Instability occurs when the transverse effective pressure acting on the perturbed magnetic tube is less than the parallel pressure: $P_{\perp 0} + B_0^2/4\pi < P_{\parallel 0}$ and $c_F^2 < 0$. In this case, transverse Alfvénic deformation of the magnetic field lines grow in time exponentially. Direction of axis adopted for the description of the flow is shown in the left bottom corner. Arrows on the axis indicate direction of the equilibrium heat fluxes, subject to linear perturbations.

and the dot denotes the temporal derivative, e.g. $\dot{\psi}(\tau) \equiv d\psi/d\tau$. Despite the fact that we have normalized perturbation harmonics to remove complex parameters due to intrinsic phase differences, Eqs. (19-26) still explicitly include complex parameters. Complex parameters are due to heat fluxes q_{\perp} and q_{\parallel} . Eq. (21) indicates that for non-trivial solutions ($P_{\perp} = S_{\perp} = v_x = b_x = b_y = 0$) pressure, velocity, magnetic field and heat flux perturbations can not be simultaneously real valued variables. Thus, heat fluxes to the anisotropic flow brake intrinsic phase difference between pressure and velocity harmonics and introduce non-removable phase differences between the harmonics of different physical quantities. Note, that incompressibility condition (Eq. 4) is already applied in the Eqs. (19-26). Here we have chosen perpendicular pressure perturbation component p_{\perp} for further analysis. Parallel pressure perturbation can be calculated from the condition $d/d\tau(\mathbf{k} \cdot \mathbf{v}) = 0$. Interestingly, non of the Eqs. (19-21) and (23-26) contain parallel heat flux perturbation (s_{\parallel}) or parallel heat flux parameter (q_{\parallel}). Thus, under considered approximation, the ODE system (19-26) can be split in two parts: parallel heat flux perturbations are driven by other perturbations (see Eq. (22)). This choice defines that only perpendicular heat flux parameter appears in further analysis. Still, we note that in present case parallel and perpendicular heat flux parameters are not independent parameters and are linked through Eqs. (10) and (16).

A. Firehose instability in static case

In the zero-shear limit ($R = 0$), k_y and thus also all coefficients in the differential equations become time-independent. Hence, we may use a spectral expansion of the linear perturbations in time $\propto \exp(i\omega\tau)$ and obtain the dispersion equation of the incompressible, anisotropic MHD system, which reads as follows:

$$[\omega^2 - (1 + \Delta\beta)k_x^2] D_0 = 0, \quad (28)$$

where

$$D_0 \equiv \omega^4 - (1 + \beta_{\perp})k^2\omega^2 + \alpha\beta_{\perp}q_{\perp}k_x k_{\perp}^2\omega + [(1 + \Delta\beta)k_x^2 + (1 + \beta_{\perp} - \alpha^2\beta_{\parallel})k_{\perp}^2] \beta_{\parallel}k_x^2. \quad (29)$$

The first obvious solution of this dispersion equation is given by the firehose mode:

$$\omega_{F\pm} = \pm c_F k_x, \quad (30)$$

where

$$c_F^2 \equiv 1 + \Delta\beta, \quad (31)$$

stands for the square of the characteristic speed of the firehose mode, when positive. It seems that kink deformations of the parallel magnetic structures that are described by the firehose mode do not feel the effect of heat fluxes (q_{\parallel} , q_{\perp}). Hence the linear stability criterion for firehose instability ($c_F^2 < 0$) can be set by the balance of the parallel and perpendicular plasma beta parameters^{4,5,36}:

$$\beta_{\parallel} > 1 + \beta_{\perp}. \quad (32)$$

The growth of linear perturbations is described by ω_{F+} or ω_{F-} , depending on whether the streamwise wave-number k_x is positive or negative, respectively.

The mechanism of the classical microscopic anisotropic MHD instability can be illustrated using a simple sketch shown in Fig. (1). Transverse perturbations of the magnetic field ($B'_{\perp} \neq 0$) can be shown as kink perturbations of the parallel magnetic structure. The response to this perturbation consists from a combined action of the parallel and perpendicular pressure and the magnetic field. If the perpendicular pressure is lower than the parallel pressure to the extent that even the magnetic field can not compensate for the kink deformation, the perturbation will grow and the instability will be developed. Interestingly, the heat fluxes (S_{\parallel} , S_{\perp}) do not affect this process. At least not in the static/uniform flow limit.

Another set of modes in the Eq. (28) are described by $D_0 = 0$ solutions: these are incompressible slow modes modified by the thermal effects. In the static case these modes are decoupled with the firehose instability and does not explicitly affect their dynamics.

B. Firehose instability in non-uniform flows

The dynamic behaviour of linear perturbations in shear flows ($R \neq 0$) are described by Eqs. (19-26). Employing the

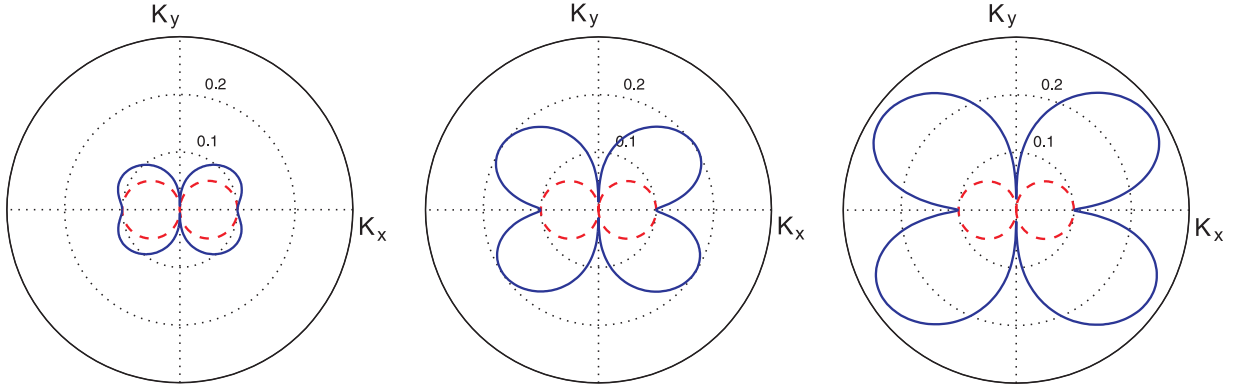


FIG. 2. The growth rate of the firehose instability as function of the angle ϕ of the wave vector with respect to the direction of the magnetic field in the shearing plane: $k_x = k_0 \cos(\phi)$ and $k_y = k_0 \sin(\phi)$ with $k_0 = 1$. Here, $\alpha = 0.5$, $\beta_{\parallel} = 2$, $q_{\perp} = 0.2$, $k_z = 1$, $c_F^2 = -0.01$ and $R = 0.05, 0.2, 0.4$ (left to right). The horizontal axis corresponds to the direction parallel and the vertical axis to the direction perpendicular to the magnetic field, respectively. The red dashed line shows the instability growth rate for static case ($R = 0$), while the solid blue line shows the velocity shear modification. It seems that an increase of the shear parameter leads to stronger instabilities for perturbations with oblique wave-numbers: $\phi \sim \pi/4$.

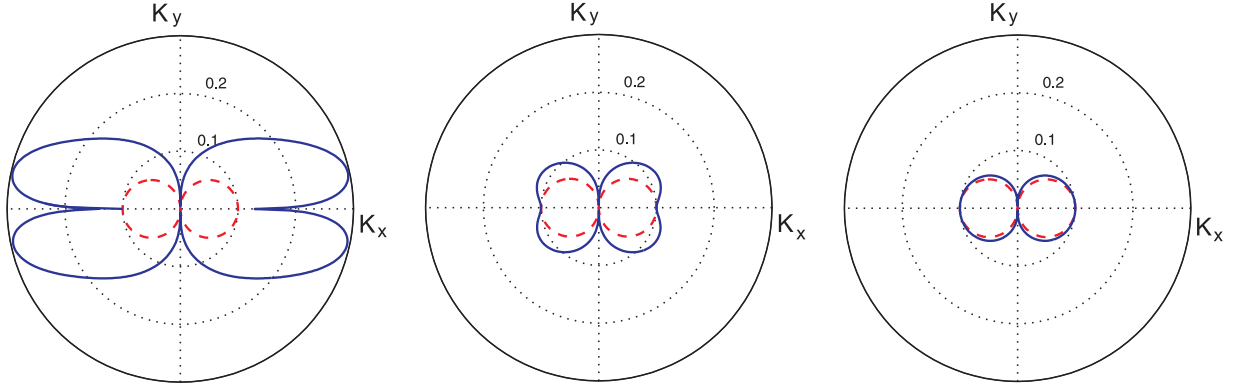


FIG. 3. The growth rate of the firehose instability as function of the angle ϕ of the wave vector with respect to the direction of the magnetic field. Here, $\alpha = 0.5$, $\beta_{\parallel} = 2$, $q_{\perp} = 0.2$, $R = 0.05$, $c_F^2 = -0.01$ and $k_z = 0, 1, 2$ (left to right). It seems that the velocity shear effect is the strongest for vertically uniform perturbations ($k_z = 0$), while small scale perturbations with $k_z > 1$ remain largely insensitive to the velocity shear effects.

low frequency limit we use the following approximation for time variation of perturbation harmonics:

$$\dot{\psi}(\mathbf{k}, \tau) \approx -i\omega(\tau)\psi(\mathbf{k}, \tau). \quad (33)$$

This limit is somewhat similar to the adiabatic limit, when temporal variations of the background are slow enough ($R \ll 1$) to introduce parameter similar to the spectral frequency $\omega(\tau)$. Such method is widely used in the adiabatic approximation, where frequency varies slower than the oscillations it describes.

$$|\dot{\omega}(\tau)| \ll \omega^2(\tau). \quad (34)$$

In our case the source of time variation of frequency (or growth rate in case of instability) is the velocity shear parameter leading to the wave-number variation in the shearing sheet limit:

$$\omega(\tau) = \omega(k_x, k_y(\tau), k_z). \quad (35)$$

Using this assumption

$$\dot{\omega}(\tau) = \frac{\partial \omega}{\partial k_y} \frac{\partial k_y(\tau)}{\partial \tau}. \quad (36)$$

and substituting Eq. (36) into the condition (34) we derive the following:

$$|\omega^2| \gg |Rk_x \frac{\partial \omega}{\partial k_y}| \quad (37)$$

In this limit, we can derive the adiabatic dispersion equation of the shear flow system and obtain:

$$[\omega^2 - (1 + \Delta\beta)k_x^2] D_0 + iRk_x k_y D_1 = 0, \quad (38)$$

where

$$D_1 \equiv (1 + \beta_{\perp})\omega^2 - \alpha\beta_{\perp}q_{\perp}k_x\omega + (\beta_{\perp}^2 - \beta_{\parallel}\beta_{\perp} - \beta_{\parallel})k_x^2, \quad (39)$$

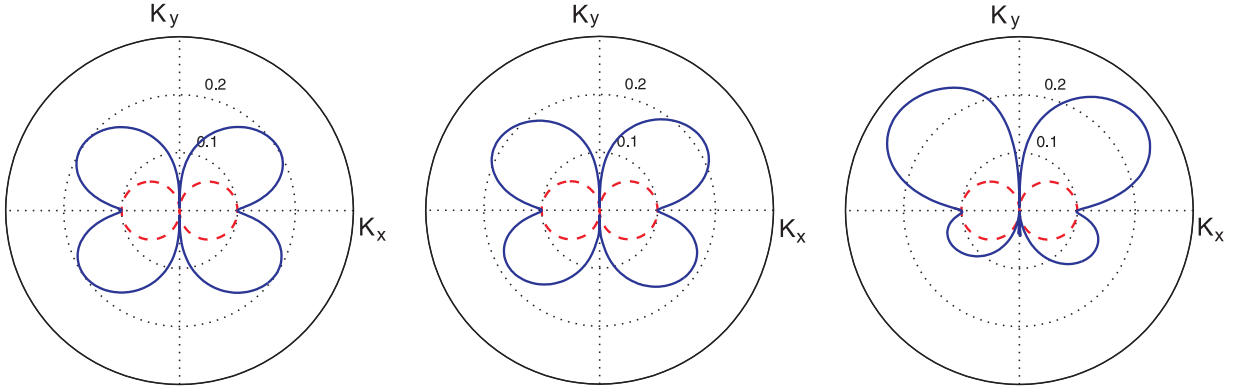


FIG. 4. The growth rate of the firehose instability as function of the angle ϕ of the wave vector with respect to the direction of the magnetic field. Here, $\alpha = 0.5$, $\beta_{\parallel} = 2$, $k_z = 1$, $c_F^2 = -0.01$, $R = 0.2$ and $q_{\perp} = 0.2, 2, 10$ (left to right). It seems that an increase of the heat flux parameter (q_{\perp}) leads to an asymmetry of the instability growth in shear flows.

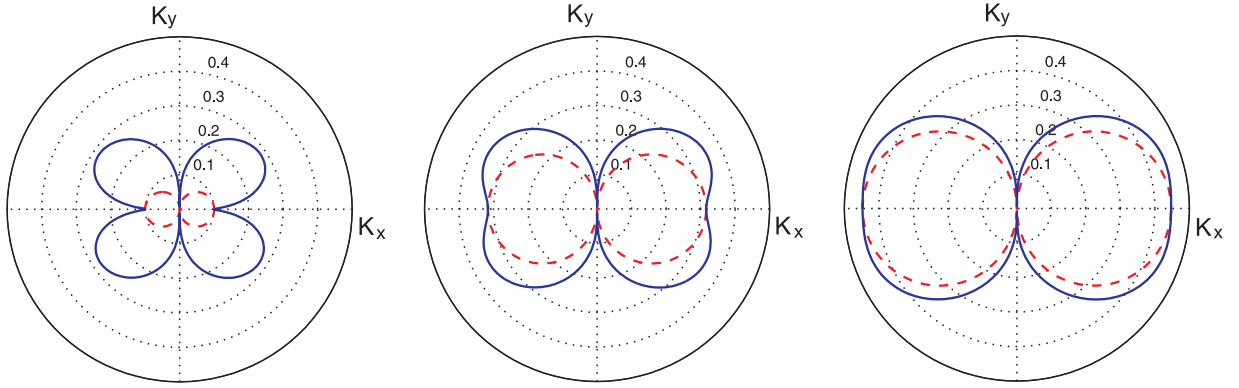


FIG. 5. The growth rate of the firehose instability as function of the angle ϕ of the wave vector with respect to the direction of the magnetic field. Here, $\alpha = 0.5$, $\beta_{\parallel} = 2$, $k_z = 1$, $R = 0.4$ and $c_F^2 = -0.01, -0.1, -0.2$ (left to right). The velocity shear effects are most profound for weakly unstable perturbations. Otherwise the growth rate of firehose instability is lower than the velocity shear parameter $\sigma^2 < R^2$ and analytic results derived within the adiabatic approximation are not valid.

shows the modification to the standard dispersion equation. The implications of the velocity shear effects on the firehose instability set by Eq. (38) are obvious. Unlike the static/uniform flow result, the firehose solutions now do depend on the velocity shear R as well as on the heat flux parameter q_{\perp} . In addition, the velocity shear effect may lead to asymmetry of the growth rates in the shearing plane (see last term of the Eq. (38)).

Modes described by Eq. (38) can be coupled due to the velocity shear of the flow. Low frequency resonance can occur between unstable firehose and MHD wave modes. Similar effect was studied in CGL limit²⁶ and it was shown that moderate shear parameter is needed for such resonant coupling to occur.

To analyze the effect of shear flow on the classical firehose mode we introduce the deviation from the static solution (30) as follows:

$$\omega = \omega_{F\pm} + R\omega_{1\pm}. \quad (40)$$

This limit can be especially useful in the low shear limit,

when $R < 1$, i.e., shearing time-scale is much longer than the Alfvén wave time-scales in the flow. Using Eq. (40) in the condition (37) and recalling that fire-hose mode frequency $\omega_{F\pm}$ does not depend on the k_y we get the applicability condition of our adiabatic approximation:

$$|\omega^2| \gg R^2 \left| k_x \frac{\partial \omega_{1\pm}}{\partial k_y} \right|. \quad (41)$$

Substituting Eq. (40) into the Eq. (38) and neglecting terms of order higher than R^2 in the low shear limit ($R < 1$), we may derive the second-order dispersion equation with respect to $\omega_{1\pm}$ as follows:

$$RA_{\pm}\omega_{1\pm}^2 + (B_{\pm} + iRC_{\pm})\omega_{1\pm} + iD_{\pm} = 0, \quad (42)$$

where

$$A_{\pm} = 4c_F^2(c_F^2 - \beta_{\parallel})k_x^2 + (3\Delta_{\pm} - 2(1 + 2\beta_{\perp}))k_{\perp}^2, \quad (43)$$

$$B_{\pm} = 2\omega_{F\pm}\Delta_{\pm}k_{\perp}^2, \quad (44)$$

$$C_{\pm} = (1 + 2\beta_{\perp} - 2\Delta_{\pm})k_x k_y, \quad (45)$$

$$D_{\pm} = -\omega_{F\pm}\Delta_{\pm}k_x k_y, \quad (46)$$

and

$$\Delta_{\pm} = \pm c_F \alpha \beta_{\perp} q_{\perp} + (1 - c_F^2)(1 + 2\beta_{\perp}) - c_F^2. \quad (47)$$

The solution of the Eq. (38) should match the standard firehose solution in the zero shear limit, i.e.

$$\omega(R=0) = \omega_{F\pm}.$$

This sets the following convergence requirement on the shear flow correction:

$$\lim_{R \rightarrow 0} (R\omega_{1\pm}) = 0. \quad (48)$$

Hence, from the two solutions of the reduced dispersion equation (42), we can choose the one obeying the asymptotic condition (48):

$$\omega_{1\pm} = \frac{B_{\pm} + iRC_{\pm}}{2RA_{\pm}} \left[-1 + \left(1 - \frac{4iRA_{\pm}D_{\pm}}{(B_{\pm} + iRC_{\pm})^2} \right)^{1/2} \right]. \quad (49)$$

Using the low shear limit ($R < 1$) we may separate the real and complex parts of the solution (49) for stable, unstable and neutrally stable firehose modes:

$$\omega = \pm c_F k_x + \delta_{1\pm} + i\sigma_{1\pm} \quad \text{when } c_F^2 > 0, \quad (50)$$

$$\omega = 2i\sigma_A \quad \text{when } c_F^2 = 0, \quad (51)$$

$$\omega = (\sigma_A + \delta_{2\pm}) + i(\pm|c_F|k_x + \sigma_{2\pm}) \quad \text{when } c_F^2 < 0, \quad (52)$$

where

$$\sigma_A \equiv R \frac{k_x k_y}{2k_{\perp}^2},$$

describes the shear flow induced transient growth of aperiodic perturbations, while the explicit forms of $\delta_{1\pm}$, $\delta_{2\pm}$, $\sigma_{1\pm}$, $\sigma_{2\pm}$ are given in the Appendix A. Applicability of the results derived in Eqs. (50-52) depend on the validity of the adiabatic approximation (see Eq. (41)). Results are valid if the growth rate of the instability is larger than the velocity shear of the flow: $\omega^2 > R^2$.

IV. DISCUSSION

In order to show the effects of different physical factors and parameters on the firehose instability, we illustrate analytic solutions given by Eq. (52).

Fig. (2) shows the comparison of the growth rates of the instability in a static case to flows with different values of the velocity shear parameter. It seems that the velocity shear effect is negligible for strictly parallel in the shear plane ($k_y = 0$) or perpendicular ($k_x = 0$) perturbations (see also Eq. (45)). However, velocity shear induces a significant boost to the instability growth rates for perturbations with wave-vectors oblique to the magnetic field.

Fig. (3) shows the growth rates of the instability in static case and sheared flows for different values of the vertical wave-number. It seems that the effect of the velocity shear is most profound on the vertically uniform perturbations with $k_z = 0$. The increase of the instability growth rates is most profound for nearly parallel perturbations with $k_x/k \lesssim 1$.

Fig. (4) shows the growth rates of the instability in flows with different heat flux parameters. Interestingly, combined action of velocity shear and heat fluxes introduces an asymmetry of the firehose instability growth in wave-number space: perturbations having a transverse component pointing in the direction of the velocity shear ($k_y > 0$), are amplified, while the perturbations with wave vectors pointing in the opposite direction ($k_y < 0$), are somewhat suppressed. Notably weaker asymmetry is introduced in the streamwise direction: perturbations in the $k_x > 0$ area grow stronger in comparison to those in the $k_x < 0$ area.

Finally Fig. (5) shows the growth rates of the instability for different values of the firehose parameter c_F^2 . The effects of the velocity shear are most profound for marginally unstable perturbations, while the violent firehose processes remain largely insensitive to the velocity shear modifications.

It seems that low frequency processes in the anisotropic flows that are marginally unstable to firehose perturbations can be significantly modified by the velocity shear as well as by heat fluxes of the MHD medium. The parallel firehose instability acquires a transverse component in shear flows and, hence, is affected by the heat fluxes. Thus the observable features of the MHD fluctuations can be significantly modified in high shear regions of anisotropic flows.

In solar and stellar winds the combined effect of the velocity shear and heat fluxes can be an additional source of turbulence and anomalous heating in rarefied magnetized outflows. The firehose instability can lead to enhanced turbulence in anisotropic MHD flows. Thus, sustained fluctuations of the solar wind can occur in areas of phase space where no instabilities are present. Therefore, observations of the fluctuations in the solar wind can be a powerful tool for analyzing the physical conditions in the wind using the stability considerations for local perturbations. Indeed, the firehose instability modified by the effects of velocity shear and heat fluxes can draw the energy of the background flow into turbulent fluctuations and, ultimately, into heat via dissipative effects which can be included in the solar/stellar models in terms of statistically proven macroscopic wave heating and pressure gradient quantities³⁷. It is also interesting to elaborate on the role of the firehose instability in the dynamics of the smaller scale flows like solar coronal jets, for which quasi-oscillatory precursors in the mean intensity variations recently have been observed³⁸ that pretend to be triggers of the instability processes occurring in coronal bright points.

Thus, the analytic solutions derived in the present paper can be used to study the features of the solar wind fluctuations by deducing the physical conditions in the outflow, such as the parameters of the heat fluxes and the azimuthal velocity shear of the radial outflow.

ACKNOWLEDGEMENTS

The work was supported by Shota Rustaveli National Science Foundation grants DI-2016-52 and FR17_609.

DATA AVAILABILITY

The data that supports the findings of this study are available within the article and its appendix.

APPENDIX: FIREHOSE SOLUTION IN NON-UNIFORM FLOWS

The modification of the firehose solutions in non-uniform flows can be described in low shear limit ($R < 1$) using Eqs. (50-52). In these equations we have introduced number of notations for the shortness of the presentation in the main text of the article. Shear flow modification in the stable ($c_F^2 > 0$) flow configuration to the real:

$$\delta_{1\pm} = \frac{k_{\perp}(t)^2}{8c_F k_x A_{\pm} \Delta_{\pm}} \left\{ M_{1\parallel} k_x^2 + \frac{|k_x \Delta_{\pm}|}{k_x \Delta_{\pm}} \sigma_A^2 [2\beta_{\perp} + 1 - 2\Delta_{\pm}]^2 \right\} \quad (\text{A1})$$

and imaginary parts of the frequency ω :

$$\sigma_{1\pm} = \sigma_A \frac{P_{1\parallel} k_x^2 + P_{1\perp} k_{\perp}(t)^2}{2A_{\pm}}, \quad (\text{A2})$$

introducing

$$\eta \equiv \alpha |c_F| \beta_{\perp} q_{\perp}, \quad (\text{A3})$$

and

$$M_{1\parallel} = 8c_F^2 \Delta_{\pm}^2 \left(-1 + \frac{|k_x \Delta_{\pm}|}{k_x \Delta_{\pm}} \right), \quad (\text{A4})$$

$$P_{1\parallel} = 4[(c_F^2 - 1)(c_F^2 - \beta_{\parallel} + 2) - \beta_{\perp} + 1], \quad (\text{A5})$$

$$P_{1\perp} = \Delta_{\pm} + \left(1 + \frac{|k_x \Delta_{\pm}|}{k_x \Delta_{\pm}} \right) [\pm\eta - 2c_F^2(1 + \beta_{\perp})] \quad (\text{A6})$$

Shear flow modification in the unstable flow configuration ($c_F^2 < 0$) to the real:

$$\delta_{2\pm} = -\sigma_A \alpha \beta_{\perp} q_{\perp} k_{\perp}(t)^2 \times \frac{(M_{2\parallel} + \eta^2 N_{2\parallel}) k_x^2 + (M_{2\perp} + \eta^2 N_{2\perp}) k_{\perp}(t)^2}{T_2}, \quad (\text{A7})$$

and imaginary parts of the frequency ω :

$$\sigma_{2\pm} = \mp \frac{\sigma_A k_{\perp}(t)^2}{2|c_F|} \times \frac{(P_{2\parallel} + \eta^2 Q_{2\parallel}) k_x^2 + (P_{2\perp} + \eta^2 Q_{2\perp}) k_{\perp}(t)^2}{T_2}. \quad (\text{A8})$$

where

$$T_2 = [\eta^2 - (2c_F^2(1 + \beta_{\perp}) - (1 + 2\beta_{\perp}))^2] \{ [4c_F^2 \times (c_F^2 - \beta_{\parallel}) k_x^2 - (6c_F^2(1 + \beta_{\perp}) - (1 + 2\beta_{\perp})) k_{\perp}(t)^2]^2 + 9\eta^2 k_{\perp}(t)^4 \},$$

$$M_{2\parallel} = 4c_F^2 (c_F^2 - \beta_{\parallel}) (-2\beta_{\perp} (-2c_F^2 + 1) - 4\beta_{\parallel} + 1) \times (2\beta_{\perp} (2c_F^2 + 4\beta_{\parallel} - 5) - 4\beta_{\parallel} + 3), \quad (\text{A10})$$

$$N_{2\parallel} = 16c_F^2 k_x^2 (c_F^2 - \beta_{\parallel}),$$

$$M_{2\perp} = 3[1 + 2(c_F^2 + \beta_{\parallel})(2c_F^2 - 1)]^2 [2(c_F^2 - 1)(c_F^2 + \beta_{\parallel}) + 1] + [6(c_F^2 + \beta_{\parallel})(c_F^2 + 2\beta_{\parallel} - 2) + 1 + 2\beta_{\perp}] \times [-2\beta_{\perp}(-2c_F^2 + 1) - 4\beta_{\parallel} + 1] [2\beta_{\perp} \times (2c_F^2 + 4\beta_{\parallel} - 5) - 4\beta_{\parallel} + 3],$$

$$N_{2\perp} = 48(c_F^2 + \beta_{\parallel})(\beta_{\parallel} - 1) + 4 + 8\beta_{\perp},$$

$$P_{2\parallel} = 4(c_F^2 - \beta_{\parallel}) c_F^2 [1 + 2(c_F^2 + \beta_{\parallel})(2c_F^2 - 1)]^2 \times [2(c_F^2 - 1)(c_F^2 + \beta_{\parallel}) + 1],$$

$$Q_{2\parallel} = 32c_F^4 (\beta_{\parallel}^2 - c_F^4),$$

$$P_{2\perp} = [6(c_F^2 + \beta_{\parallel})(c_F^2 + 2\beta_{\parallel} - 2) + 1 + 2\beta_{\perp}] \times [1 + 2(c_F^2 + \beta_{\parallel})(2c_F^2 - 1)]^2 (2c_F^2 - 1)(c_F^2 + \beta_{\parallel}) + 1, \\ Q_{2\perp} = 12\eta^2 + 3([2\beta_{\perp}(-2c_F^2 + 1) - 4\beta_{\parallel} + 1][2\beta_{\perp} \times (c_F^2 + 2\beta_{\parallel} - 2) + 1 + 2\beta_{\perp}](c_F^2 + \beta_{\parallel}) c_F^2 + 4\beta_{\parallel} - 5) - 4\beta_{\parallel} + 3] - 8[6(c_F^2 + \beta_{\parallel})(c_F^2 + 2\beta_{\parallel} - 2) + 1 + 2\beta_{\perp}] \times (c_F^2 + \beta_{\parallel}) c_F^2.$$

REFERENCES

- ¹C. L. Longmire, M. N. Rosenbluth, Phys. Rev. **103**, 507 (1956).
- ²A. A. Vedenov, R. Z. Sagdeev, R. Z. Sov. Phys. Dokl. **3**, 278 (1958).
- ³S. Chandrasekhar, A. N. Kaufman, K. M. Watson, Proc. Roy. Soc. Lon. A **245**, 435 (1958).
- ⁴E. N. Parker, Phys. Rev. **109**, 1874 (1958).
- ⁵A. A. Vedenov, E. P. Velikhov, R. Z. Sagdeev, Sov. Usp. Fiz. Nauk **73**, 701 (1961).
- ⁶B. M. Shergelashvili, S. Poedts, A. D. Pataraya, ApJL **642**, L73 (2006)
- ⁷M. Sarfraz, P. H. Yoon, S. Saeed, G. Abbas, and H. A. Shas, Phys. Plasmas **24**, 012907 (2017).
- ⁸P. Astfalk, and F. Jenko, J. Geophys. Res. Space Phys. **121**, 2842 (2016).
- ⁹M. S. dos Santos, L. F. Ziebell, and R. Gaelzer, Phys. Plasmas **21**, 112102 (2014).
- ¹⁰M. Lazar, S. Poedts, R. Schlickeiser, D. Ibscher Solar Phys. **289**, 369 (2014).
- ¹¹R. Schlickeiser, and T. Skoda, Astrophys. J. **716**, 1596 (2010).
- ¹²M. Lazar, and S. Poedts Astron. Astrophys. **494**, 311 (2009).
- ¹³M. S. Rosin, A. A. Schekochihin, F. Rincon, and S. C. Cowley, Mon. Not. R. Astron. Soc. **413**, 7 (2011).

- ¹⁴L.-N. Hau, and B.-J. Wang, *Nonlin. Proc. Geophys.* **14**, 557 (2007).
- ¹⁵B.-J. Wang, and L.-H. Hau, *J. Geophys. Res.* **108**, 1463 (2003).
- ¹⁶C. H. K. Chen, L. Matteini, A. A. Schekochihin, M. L. Stevens, C. S. Salem, B. A. Maruca, M. W. Kunz, and S. D. Bale, *Astrophys. J.* **825**, L26 (2016).
- ¹⁷D. Ibscher, and R. Schlickeiser, *Phys. Plasmas* **21**, 022120 (2014).
- ¹⁸L. Matteini, S. Landi, M. Velli, and W. H. Matthaeus, *Astrophys. J.* **763**, 142 (2013).
- ¹⁹R. Schlickeiser, M. J. Michno, D. Ibscher, M. Lazar, and T. Skoda, *Phys. Rev. Letters* **107**, 201102 (2011).
- ²⁰S. D. Bale, J. C. Kasper, G. G. Howes, E. Quartaert, C. Salem, and D. Sundkvist, *Phys. Rev. Letters* **103**, 211101 (2009).
- ²¹A. A. Schekochihin, S. C. Cowley, R. M. Kulsrud, M. S. Rosin and T. Heinemann, *Phys. Rev. Letters* **100**, 081301 (2008).
- ²²J. Seough, P. H. Yoon, and J. Hwang *Phys. Plasmas* **22**, 012303 (2015).
- ²³M. W. Kunz, A. A. Schekochihin, and J. M. Stone, *Phys. Rev. Letters* **112**, 205003 (2014).
- ²⁴B. M. Shergelashvili, C. Maes, S. Poedts, T. V. Zaqarashvili, *Phys. Rev. E*, **76**, 046404 (2007).
- ²⁵G. F. Chew, M. L. Goldberg and F. E. Low, *Proc. R. Soc. A* **236**, 2 (1956).
- ²⁶G. D. Chagelishvili, A. D. Rogava, and D. Tsiklauri, *Phys. Plasmas* **4**, 1182 (1997).
- ²⁷P. Hunana, and G. P. Zank, *Astrophys. J.* **839**, 13 (2017).
- ²⁸V. Oraevskii, R. Chodura, W. Feneberg, *Plasma Phys.* **10**, 819 (1968)
- ²⁹N. S. Dzhililov, V. D. Kuznetsov, and J. Staude, *Astron. Astrophys.* **489**, 769 (2008).
- ³⁰H. Grad, *Commun. Pure Appl. Math.* **2**, 331 (1949).
- ³¹V. D. Kuznetsov, and N. S. Dzhililov, *Plasma Phys. Rep.* **35**, 962 (2009).
- ³²V. D. Kuznetsov, and N. S. Dzhililov, *Plasma Phys. Rep.* **36**, 788 (2010).
- ³³N. S. Dzhililov, V. D. Kuznetsov, and J. Staude, *Contrib. Plasma Phys.* **51**, 621 (2011).
- ³⁴E. S. Uchava, B. M. Shergelashvili, A. G. Tevzadze, and S. Poedts, *Phys. Plasmas* **21**, 082902 (2014).
- ³⁵R. F. Ismayilli, N. S. Dzhililov, B. M. Shergelashvili, S. Poedts, M. Sh. Pirgulyev, *Phys. Plasmas* **25**, 062903 (2018).
- ³⁶A. Evangelias and G. N. Throumoulopoulos, *J. Plasma Phys.*, **86**, 905860312 (2020).
- ³⁷B. M. Shergelashvili, H. Fichtner, *ApJ*, **752**, 142 (2012).
- ³⁸S. R. Bagashvili, B. M. Shergelashvili, D. R. Japaridze, V. Kukhianidze, S. Poedts, T. V. Zaqarashvili, M. L. Khodachenko, P. De Causmaecker, *ApJL*, **855**, L21 (2018).